Journal of Solid Mechanics Vol. 14, No. 3 (2022) pp. 312-331
DOI: 10.22034/jsm.2021.1908516.1646

Research Paper

Transient Dynamic Analysis of Grid-Stiffened Composite Conical Shells

M. Zamani, A. Davar *, M. Heydari Beni, J. Eskandari Jam

Faculty of Materials and Manufacturing Technologies, Malek Ashtar University of Technology, Tehran, Iran

Received 28 March 2022; accepted 27 May 2022

ABSTRACT

In this study, the transient dynamic analysis of grid-stiffened composite conical shells is discussed. The transient dynamic response of the composite conical shell with simply supported boundary conditions under the lateral impact load, which is applied extensively and uniformly on a certain surface, is obtained using the convolution integral and based on the method of addition of modes. The validation of the obtained results has been done with the help of references and ABAQUS finite element software. The effects of various parameters such as fiber angle, geometric ratios, type, etc. have been investigated in forced vibrations. Finally, the effect of reinforcing the conical shell with the help of grid-stiffened structures has been studied.

Keywords : Dynamic Analysis; Grid-stiffened; Composite Conical Shells.

1 INTRODUCTION

MOST composite structures are weak against impact loads. Applying a small impact load can lead to major damage and reduce the stiffness of the composite structure. Numerous studies have been conducted to investigate the dynamic response under low-velocity and high-velocity impact loads. Dobyns [1] presented an analysis of the motion of a multilayer plate under sinusoidal, stepped, and triangular impacts. Ramkumar and Chen [2] compared analytical and experimental solutions for predicting scaling and the starting point for the failure of fibers under low-velocity impact loads. Cederbaum and Heller [3] studied the dynamic response of a single-layer orthotropic cylindrical shell under local impact loads using thick-walled theory. Reddy and Khdeir [4] studied the transient response of the cylindrical shell using the high-order shear deformation theory. Davar et al. [5, 6] also examined the transient dynamic response of the composite cylinder under axial compression load and the optimization of the response. However, no research has been done so far on the transient dynamic response of conical shells. Grid-stiffened cylindrical and conical shells are shells with stiffeners inside, outside, or both sides of the shell. These stiffeners significantly increase the load-bearing capacity of the shells without much weight gain. The appropriate stiffener is selected based on the type of application, loading status, cost, and other factors [7-8]. The number of papers dealing with the mechanical behavior of composite cylinders with inclined stiffeners is small,

*Corresponding author. Tel.: +98 21 22970203.
E-mail address: a_davar@mut.ac.ir, davar78@gmail.com (A. Davar)

and most research in this field is related to cylinders stiffened with longitudinal and peripheral ribs. Kidan et al. [9,10] obtained the buckling load of composite cylinders with inclined and horizontal stiffeners by developing a method for determining the stiffness parameters equivalent to a grid-stiffened composite cylindrical shell. Also, Yazdani [11] and Yazdani and Rahimi [12] conducted an experimental study on the buckling behavior of composite cylindrical shells with an inclined stiffener. They also studied the effect of the number of spiral ribs and the changes in the type of stiffening grid on the buckling loads of these shells [13,14]. Rahimi et al. used a finite element method to investigate the effect of the cross-sectional profile of the stiffener on the buckling strength of composite cylindrical shells [15]. Recently, Hemmatnejad [16] has calculated the free vibrations of grid-stiffened cylindrical shells with inclined ribs based on the first-order shear deformation theory. He also studied the effect of changes in shell thickness and boundary conditions on shell frequencies. However, so far, no research has been done on the dynamic response of grid-stiffened (cylindrical and conical) shells, and free vibrations of conical shells with grid-stiffened structure. Methods of research and experiments have shown that many composite structures are weak against impact loads [17]. Applying a small impact load may cause a large deformation and a decrease in the strength of the composite structure. Therefore, in designing the desired composite structures, the dynamic response of the structure should be examined in detail. This chapter discusses the transient dynamic response of composite conical shells with simply supported boundary conditions, under the lateral impulse load applied to the outer surface of the conical shell.

To examine the dynamic response of the shell, the results of the analysis of free vibrations (i.e., natural frequencies and the shape of normalized modes), which were calculated in the previous chapter, have been used. Finally, the changes in shell displacement in the three *x.Θ.z* directions over time have been calculated using Laplace transform and based on the mode-superposition technique. Here it is necessary to define two characteristics of the desired impulse load to explain the problem statement: The location and dimensions of the applied impulse load surface on the shell changes in load value over time.

2 THE LOCATION OF THE IMPULSE LOAD AND THE DIMENSIONS OF THE APPLIED LOAD SURFACE ON THE SHELL

The impact load of $f(t)$ on a rectangular surface is applied to the surface of a conical shell with an average radius of $R = \frac{a+b}{2}$ and a length L according to Fig. 1. It is assumed that the load is applied uniformly on the desired surface. According to Fig. 1, the coordinates of the midpoint of this surface are defined as follows:

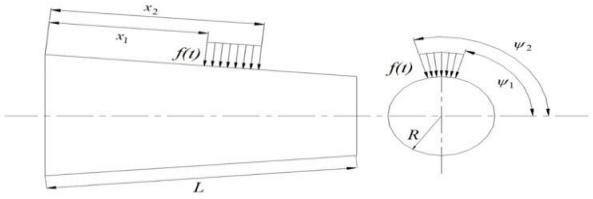

Fig.1
Load applied on a rectangular surface.

$$x_L = \frac{x_1 + x_2}{2} \tag{1}$$

$$\theta_L = \frac{\psi_1 + \psi_2}{2} \tag{2}$$

and the dimensions of the applied load surface are defined as follows:

$$R(\psi_2 - \psi_1) = 2l_1 \tag{3}$$

$$x_2 - x_1 = 2l_2 \tag{4}$$

Therefore, for ease of definition, the location and dimensions of the applied load surface are referred to as follows:

Dimensions of the applied load surface: $2l_1 * 2l_2$

Coordinates of the location of the applied load: $\begin{cases} x = x_L \\ \theta = \theta_L \end{cases}$

3 CHANGES IN LOAD VALUE OVER TIME

The load applied on the surface is in the form of an impulse or pulse, i.e. it is applied on the shell surface as a time-varying pressure. The diagram of the pressure in terms of time is shown in Fig. 2 for the types of the studied pulses. In these diagrams, t_1 is the end time of the load applying, and f_0 is the maximum amount of the applied pressure. One of the cases in which time-varying pressure is produced is the pressure caused by the explosion, which can be considered as a saw-tooth pulse.

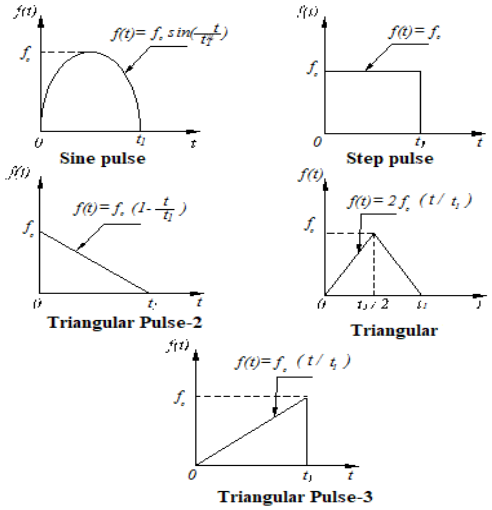

Fig.2
Pressure diagram of different pulses over time.

4 EQUATIONS GOVERNING THE FORCED VIBRATIONS OF COMPOSITE CONICAL SHELLS

In the section of free vibration analysis, time-varying external stimuli were omitted in defining the relations related to the forces p_x , p_y , and p_z . However, to analyze forced vibrations, phrases related to time-varying external stimuli should be considered as follows [18]:

$$\begin{cases} p_x = -I_1 \dfrac{\partial^2 u}{\partial t^2} + q_x(x,\theta,t) \\ p_y = -I_1 \dfrac{\partial^2 v}{\partial t^2} + q_y(x,\theta,t) \\ p_z = -I_1 \dfrac{\partial^2 w}{\partial t^2} + q_z(x,\theta,t) \end{cases} \tag{5}$$

where q_x , q_y , and q_z are time-varying external stimuli in the directions of z and $\theta.x$, respectively, and are defined according to the boundary conditions. Considering that according to the applied load definition, the external stimulus is applied only in the z-direction and there is no external stimulus in the directions of x and θ, we have:

$$\begin{cases} q_x(x,\theta,t)=0 \\ q_y(x,\theta,t)=0 \\ q_z(x,\theta,t)\neq 0 \end{cases} \tag{6}$$

5 TRANSIENT DYNAMIC RESPONSE OF SIMPLY SUPPORTED COMPOSITE CONICAL SHELL

Because of the importance of the subject, here the dynamic response of the simply supported composite conical shell under axial load is investigated. The equations of motion of the simply supported composite conical shell are expressed as follows [18]:

$$\begin{bmatrix} L_{11} & L_{12} & L_{13} \\ L_{21} & L_{22} & L_{23} \\ L_{31} & L_{32} & L_{33} \end{bmatrix} \begin{Bmatrix} u \\ v \\ w \end{Bmatrix} = \begin{Bmatrix} I_1 R \dfrac{\partial^2 u}{\partial t^2} \\ I_1 R \dfrac{\partial^2 v}{\partial t^2} \\ I_1 R \dfrac{\partial^2 w}{\partial t^2} - q_z(x,\theta,t)R \end{Bmatrix} \tag{7}$$

Considering the simply supported boundary conditions, the external stimulation is defined as follows [18]:

$$q_z(x,\theta,t)=Q_z(x,\theta)f(t)=[\sum_{m=1}^{\infty}\sum_{n=0}^{\infty}P_{mn}\ \sin\frac{m\pi x}{L}\cos n\theta]f(t) \tag{8}$$

In this relation, P_{mn} are the Fourier coefficients that depend on how the load is applied. To calculate these coefficients, the sides of Eq. (7) are multiplied by $\sin\dfrac{m\pi x}{L}\cos n\theta$ and the integrals are taken from the sides. As a result, we will have:

$$\begin{aligned} &n=0,\ P_{m0}=\frac{2}{\pi L}\int_0^L\int_{-\pi}^{\pi} Q_z(x,\theta)\sin\frac{m\pi x}{L}\ dx\,d\theta \\ &n>0,\ P_{mn}=\frac{2}{\pi L}\int_0^L\int_{-\pi}^{\pi} Q_z(x,\theta)\sin\frac{m\pi x}{L}\cos n\theta\,dx\,d\theta \end{aligned} \tag{9}$$

To simplify the calculations, it is assumed that the amount of load is uniform and equal to one $Q_z(x,\theta)=1$. By integrating, we have:

$$\begin{aligned} &n=0,\ P_{m0}=\frac{2}{m\pi^2}(\frac{1}{x_1}\cos\frac{m\pi x_1}{L}-\frac{1}{x_2}\cos\frac{m\pi x_2}{L}) \\ &n>0,\ P_{mn}=\frac{2}{m\,n\,\pi^2}(\sin n\psi_2-\sin n\psi_1)(\frac{1}{x_1}\cos\frac{m\pi x_1}{L}-\frac{1}{x_2}\cos\frac{m\pi x_2}{L}) \end{aligned} \tag{10}$$

and in a special case where the midpoint of the surface of the load is in ($x_L=L/2$, $\theta_L=0$), using the expansion of trigonometric functions, after simplification we have [18]:

$$\begin{aligned} &n=0,\ \ P_{m0}=\frac{8l_1}{\pi^2\,m\,R}\sin\frac{m\pi}{2}\sin\frac{m\pi l_2}{L} \\ &n>0,\ \ P_{mn}=\frac{8}{\pi^2\,m\,n}\sin\frac{m\pi}{2}\sin\frac{m\pi l_2}{L}\sin\frac{n l_1}{R} \end{aligned} \tag{11}$$

By substituting the assumed changes in the equilibrium Eqs. (7), we have:

$$\begin{bmatrix} L_{11} & L_{12} & L_{13} \\ L_{21} & L_{22} & L_{23} \\ L_{31} & L_{32} & L_{33} \end{bmatrix} \begin{Bmatrix} \overline{A}_{mn} \\ \overline{B}_{mn} \\ \overline{C}_{mn} \end{Bmatrix} T_{mn}(t) = \begin{Bmatrix} \ddot{T}_{mn}(t) I_1 R \overline{A}_{mn} \\ \ddot{T}_{mn}(t) I_1 R \overline{B}_{mn} \\ \ddot{T}_{mn}(t) I_1 R \overline{C}_{mn} - q_z(x,\theta,t) R \end{Bmatrix} \tag{12}$$

Using the free vibration relations ($T_{mn}(t) = e^{i\omega_{mn}t}$), the right side of the above relation can be substituted as follows:

$$\begin{bmatrix} L_{11} & L_{12} & L_{13} \\ L_{21} & L_{22} & L_{23} \\ L_{31} & L_{32} & L_{33} \end{bmatrix} \begin{Bmatrix} \overline{A}_{mn} \\ \overline{B}_{mn} \\ \overline{C}_{mn} \end{Bmatrix} T_{mn}(t) = -\omega_{mn}^2 T_{mn}(t) I_1 R \begin{Bmatrix} \overline{A}_{mn} \\ \overline{B}_{mn} \\ \overline{C}_{mn} \end{Bmatrix} \tag{13}$$

By substituting relation 11 by relation 12, the following relation is obtained [18]:

$$\begin{aligned} -\omega_{mn}^2 T_{mn}(t)\, I_1 \overline{A}_{mn} &= \ddot{T}_{mn}(t)\, I_1 \overline{A}_{mn} \\ -\omega_{mn}^2 T_{mn}(t)\, I_1 \overline{B}_{mn} &= \ddot{T}_{mn}(t)\, I_1 \overline{B}_{mn} \\ -\omega_{mn}^2 T_{mn}(t)\, I_1 \overline{C}_{mn} &= \ddot{T}_{mn}(t)\, I_1 \overline{C}_{mn} - q_z(x,\theta,t) \end{aligned} \tag{14}$$

The sides of the relationship 14 are multiplied by $\overline{A}_{mn}$, $\overline{B}_{mn}$, and $\overline{A}_{mn}$, respectively. After adding the sides of the relation, we have:

$$\ddot{T}_{mn}(t) I_1 (\overline{A}_{mn}^2 + \overline{B}_{mn}^2 + \overline{C}_{mn}^2) + \omega_{mn}^2 T_{mn}(t) I_1 (\overline{A}_{mn}^2 + \overline{B}_{mn}^2 + \overline{C}_{mn}^2) = \overline{C}_{mn} q_z(x,\theta,t) \tag{15}$$

By factoring and integrating with respect to x and θ from the sides of the above equation, an ordinary second-order differential equation in terms of time is obtained as follows:

$$\ddot{T}_{mn}(t) + \omega_{mn}^2 T_{mn}(t) = G_{mn}(t) \tag{16}$$

The expression on the right side of the above equation is called generalized forces and is obtained as follows:

$$G_{mn}(t) = \frac{\int_0^L \int_{-\pi}^{\pi} \overline{C}_{mn} q_z(x,\theta,t)\, dx\, d\theta}{\int_0^L \int_{-\pi}^{\pi} I_1 (\overline{A}_{mn}^2 + \overline{B}_{mn}^2 + \overline{C}_{mn}^2)\, dx\, d\theta} \tag{17}$$

The denominator of the above fraction is called the normalized mass [18]. By substituting (7) in the numerator and denominator of the fraction on the other side of Eq. (17) and by integrating, we have:

$$G_{mn}(t) = \frac{P_{mn} C_{mn} \pi \frac{L}{2}}{I_1 \pi \frac{L}{2} (A_{mn}^2 + B_{mn}^2 + C_{mn}^2)} \tag{18}$$

By considering:

$$N_{mn} = I_1 (A_{mn}^2 + B_{mn}^2 + C_{mn}^2) \tag{19}$$

We have:

$$\ddot{T}_{mn}(t)+\omega_{mn}^2 T_{mn}(t)=\frac{P_{mn}C_{mn}f(t)}{N_{mn}} \tag{20}$$

The Laplace transform is obtained from the sides of Equation (20):

$$\mathrm{L}(\ddot{T}_{mn}(t)+\omega_{mn}^2 T_{mn}(t))=\mathrm{L}(\frac{P_{mn}C_{mn}f(t)}{N_{mn}}) \tag{21}$$

Assuming that $t\geq 0$, we have[18]:

$$s^2T_{mn}(s)-sT_{mn}(0)-\dot{T}_{mn}(0)+\omega_{mn}^2T_{mn}(s)=\frac{P_{mn}C_{mn}F(s)}{N_{mn}} \tag{22}$$

where $T_{mn}(s)=\mathrm{L}(T_{mn}(t))$, $F(s)=\mathrm{L}(f(t))$. Assuming the initial zero conditions $(T_{mn}(0)=\dot{T}_{mn}(0)=0)$.

We have:

$$s^2T_{mn}(s)+\omega_{mn}^2T_{mn}(s)=\frac{P_{mn}C_{mn}F(s)}{N_{mn}} \tag{23}$$

By simplification, we have:

$$T_{mn}(s)=\frac{P_{mn}C_{mn}F(s)}{(s^2+\omega_{mn}^2)N_{mn}} \tag{24}$$

By multiplying the numerator and denominator by ω_{mn}, we have:

$$T_{mn}(s)=\frac{P_{mn}C_{mn}}{N_{mn}\omega_{mn}}\frac{\omega_{mn}}{(s^2+\omega_{mn}^2)}F(s) \tag{25}$$

By taking the inverse Laplace transform from both sides of the above relation and using Convolution theorem, we have [18]:

$$T_{mn}(t)=\frac{P_{mn}C_{mn}}{N_{mn}\omega_{mn}}\int_0^t f(\tau)\sin\omega_{mn}(t-\tau)d\tau \tag{26}$$

Finally, the temporal response of the composite cylindrical shell with simply-supported boundary conditions, under the defined impact load, is obtained based on the mode-superposition theory as follows:

$$\begin{aligned}
u&=\sum_{m=1}^{\infty}\sum_{n=0}^{\infty}\frac{P_{mn}C_{mn}}{N_{mn}\omega_{mn}}A_{mn}\cos\frac{m\pi x}{L}\cos n\theta\int_0^t f(\tau)\sin\omega_{mn}(t-\tau)d\tau\\
v&=\sum_{m=1}^{\infty}\sum_{n=0}^{\infty}\frac{P_{mn}C_{mn}}{N_{mn}\omega_{mn}}B_{mn}\sin\frac{m\pi x}{L}\sin n\theta\int_0^t f(\tau)\sin\omega_{mn}(t-\tau)d\tau\\
w&=\sum_{m=1}^{\infty}\sum_{n=0}^{\infty}\frac{P_{mn}C_{mn}^2}{N_{mn}\omega_{mn}}\sin\frac{m\pi x}{L}\cos n\theta\int_0^t f(\tau)\sin\omega_{mn}(t-\tau)d\tau
\end{aligned} \tag{27}$$

6 THE TEMPORAL FUNCTION OF THE SHELL DISPLACEMENT RESPONSE

As shown in Eq. (26), the shell displacement response consists of a spatial function and a temporal function. The spatial function of the response is the same as the mode shape, and its temporal function is the convolution integral, which must be calculated according to the type of pulse. The convolution integral for the various pulses are calculated below [19 and 20]:

Step pulse

$$\begin{cases} f(t)=f_0\,,\ 0\le t\le t_1 \\ f(t)=0,\ t>t_1 \end{cases}$$

$$\int_0^t f(\tau)\sin\omega_{mn}(t-\tau)d\tau=\begin{cases} \dfrac{f_0}{\omega_{mn}}(1-\cos\omega_{mn}t)\ , & 0\le t\le t_1 \\ \dfrac{f_0}{\omega_{mn}}[\cos\omega_{mn}(t-t_1)-\cos\omega_{mn}t]\ , & t>t_1 \end{cases} \tag{28}$$

Sine pulse

$$\begin{cases} f(t)=f_0\sin(\dfrac{\pi t}{t_1}),\ 0\le t\le t_1 \\ f(t)=0,\ t>t_1 \end{cases}$$

$$\int_0^t f(\tau)\sin\omega_{mn}(t-\tau)d\tau=\begin{cases} \dfrac{f_0 t_1[\pi\sin(\omega_{mn}t)-\omega_{mn}t_1\sin(\pi t/t_1)]}{(\pi^2-t_1^2\omega_{mn}^2)}\ ,\ 0\le t\le t_1 \\ \dfrac{f_0 t_1\pi[\sin(\omega_{mn}t)+\sin\omega_{mn}(t-t_1)]}{(\pi^2-t_1^2\omega_{mn}^2)}\ ,\ t>t_1 \end{cases} \tag{29}$$

Triangular pulse-1

$$\begin{cases} f(t)=2f_0(\dfrac{t}{t_1}),\ 0\le t\le t_1/2 \\ f(t)=-4f_0(t-t_1/2)/t_1\,,\ t_1/2<t\le t_1 \\ f(t)=2f_0(t-t_1)/t_1\,,\ t>t_1 \end{cases}$$

$$\int_0^t f(\tau)\sin\omega_{mn}(t-\tau)d\tau=\begin{cases} \dfrac{2f_0}{\omega_{mn}}\left[\dfrac{t}{t_1}-\dfrac{\sin(\omega_{mn}t)}{\omega_{mn}t_1}\right],\ 0\le t\le t_1/2 \\ \dfrac{2f_0}{\omega_{mn}}\left[1-\dfrac{t}{t_1}-\dfrac{\sin(\omega_{mn}t)}{\omega_{mn}t_1}+\dfrac{2\sin\omega_{mn}(t-t_1/2)}{\omega_{mn}t_1}\right],\ t_1/2<t\le t_1 \\ \dfrac{2f_0}{\omega_{mn}}\left[-\dfrac{\sin(\omega_{mn}t)}{\omega_{mn}t_1}+\dfrac{2\sin\omega_{mn}(t-t_1/2)}{\omega_{mn}t_1}-\dfrac{\sin\omega_{mn}(t-t_1)}{\omega_{mn}t_1}\right],\ t>t_1 \end{cases} \tag{30}$$

Triangular pulse-2

$$\begin{cases} f(t)=f_0(1-t/t_1),\ 0\le t\le t_1 \\ f(t)=0,\ t>t_1 \end{cases}$$

$$\int_0^t f(\tau)\sin\omega_{mn}(t-\tau)d\tau=\begin{cases} \dfrac{f_0}{\omega_{mn}}[1-\cos\omega_{mn}t+\dfrac{\sin(\omega_{mn}t)}{\omega_{mn}t_1}-t/t_1\ ,\ 0\le t\le t_1 \\ f_0[\dfrac{-1}{\omega_{mn}}\cos\omega_{mn}t+\dfrac{2\cos\omega_{mn}(t-t_1)\sin\omega_{mn}(t_1/2)}{\omega_{mn}^2\,t_1}]\ ,\ t>t_1 \end{cases} \tag{31}$$

Triangular pulse-3

$$\begin{cases} f(t) = f_0(\frac{t}{t_1}),\ 0 \le t \le t_1 \\ f(t) = 0,\ t > t_1 \end{cases}$$

$$\int_0^t f(\tau)\sin\omega_{mn}(t-\tau)d\tau = \begin{cases} \frac{f_0}{\omega_{mn}t_1}[t - \frac{\sin(\omega_{mn}t)}{\omega_{mn}}],\ 0 \le t \le t_1 \\ \frac{f_0}{\omega_{mn}t_1}[\frac{\sin\omega_{mn}(t-t_1)}{\omega_{mn}} + t_1\cos\omega_{mn}(t-t_1) - \frac{\sin(\omega_{mn}t)}{\omega_{mn}}],\ t > t_1 \end{cases} \quad (32)$$

Continuous pulse

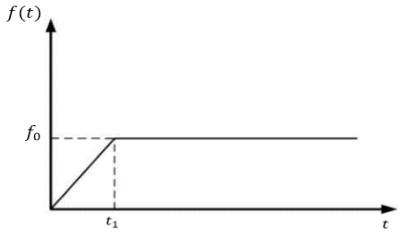

Fig.3
Continuous pulse.

$$\begin{cases} f(t) = f_0(\frac{t}{t_1}),\ 0 \le t \le t_1 \\ f(t) = 0,\ t > t_1 \end{cases}$$

$$\int_0^t f(\tau)\sin\omega_{mn}(t-\tau)d\tau = \begin{cases} \frac{f_0(t/t_1) - \sin(\omega_{mn}t)}{\omega_{mn}t_1},\ 0 \le t \le t_1 \\ \frac{f_0(1+\sin\omega_{mn}(t-\tau) - \sin(\omega_{mn}t)) - \sin(\omega_{mn}t)}{\omega_{mn}t_1},\ t > t_1 \end{cases} \quad (33)$$

7 MODELING AND ANALYSIS IN ABAQUS SOFTWARE

To validate the analysis of forced vibrations of conical shells and grid-stiffened conical shells, this structure is modeled in ABAQUS software and modal analysis and analysis of radial displacement changes over time are performed by this software. Here is how to model and analyze a composite conical shell.

8 MODELING AND ANALYSIS TO CALCULATE THE NATURAL FREQUENCIES OF THE GRID-STIFFENED CONICAL SHELL

Geometry. In order to model the conical shell, the method of rotation around the cone axis is used and the geodetic path is selected for inclined stiffeners.

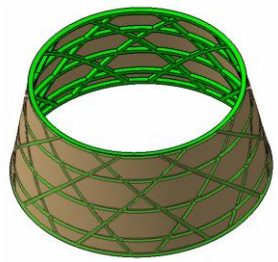

Fig.4
Grid-stiffened conical shell model.

Material type. Composites are linear elastic materials. For two-dimensional composites (plate stress) in which 6 components of elastic constants are given, the following method is done to determine the properties of elastic materials (the property section): Mechanical⟶Elasticity⟶Elastic: Type: Lamina.

Determining the properties of shells and stiffeners and the direction of fibers is done with the help of the composite Lay-Up module.

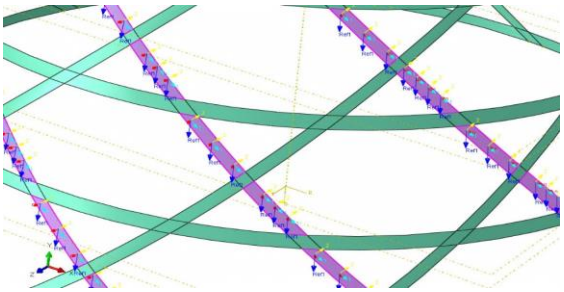

Fig.5
Determining the direction of the fibers.

Force and boundary conditions. Simply-supported boundary conditions based on the cylindrical coordinate system are applied to the structure. Also, the Amplitude section is used to check the transient dynamic loading to report force changes over time to the software.

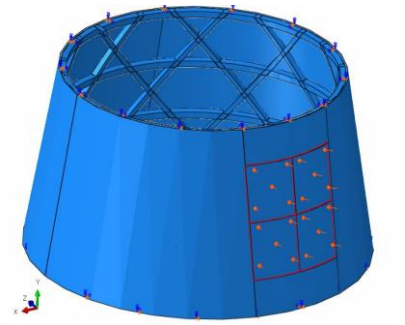

Fig.6
How to apply loading and boundary conditions on the model.

Meshing. The S4R element is used for meshing.

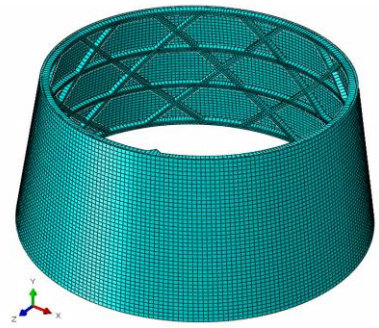

Fig.7
Meshing of a composite grid-stiffened conical model.

9 INVESTIGATING THE RESULTS OF FORCED VIBRATIONS OF THE COMPOSITE CONICAL SHELL WITH A SIMPLE SUPPORT

In computer code, the number of modes ($m \times n$) must be selected to obtain the answer. The number of m and n must be such that the answer is convergent [17]. Fig. 8 shows the convergence of the response for different $m \times n$. After observing the convergence of the answers after $m = 20$ and $n = 30$ and also to reduce the calculation time, the number of modes $m = 20$ and $n = 30$ were selected. In all cases, the time of applying the impulse load from zero to t_1 is equal to the natural period of the structure (i.e. the reverse of the base frequency in Hertz). The coordinates of the

place of applying the load (x_L ϕ_L) and the coordinates of the point on the shell where the temporal response is calculated are in the position ($x = L/2$. $\varphi = 0$), except for the cases specified .The load applied to the shell is also indicated by F_0 (force) and f_0 (pressure).

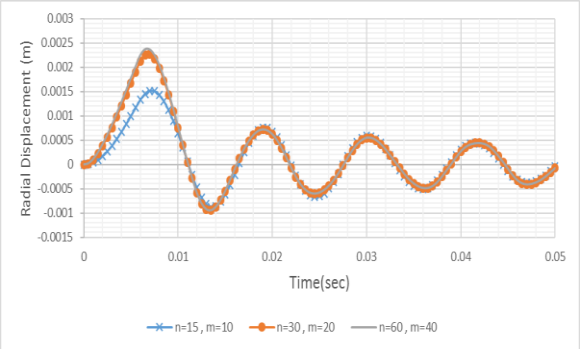

Fig.8
Investigating the convergence of the temporal response of the shell with simply-supported boundary conditions $a = 1m$. $L = 1m$. $h = 2mm$, CFRP material, lay-up [0/90/0/90/0/90], load applying area $2l_1 \times 2l_2 = 5 \times 5\ cm^2$, triangular pulse type 1, $f_0 = 25kPa$, 60˚-vertex angles.

10 VERIFICATION OF DYNAMIC RESPONSE WITH REFERENCES AND FINITE ELEMENT SOFTWARE

To verify the results obtained from the transient dynamic analysis, in Figs. 9 and 10, the results obtained from the present method for changes in radial displacement (radial displacement is the same as the amplitude of vibration in the radial direction perpendicular to the edge) in terms of time for the simply-supported conical shell are compared with the reference answer and ABAQUS finite element software. Since there was no reference to investigate the dynamic response of the conical shell at the time of writing this paper, a reference that examined the specific state of the conical geometry, the cylinder, was selected for comparison, as shown in Fig. 11. Then, to validate the dynamic response of conical geometry, the answer obtained from the computer program was compared with the answer obtained from Abacus finite element software. As shown in the figures, the answers are well matched. The reason for the slight difference in the diagrams is the difference in the theories used.

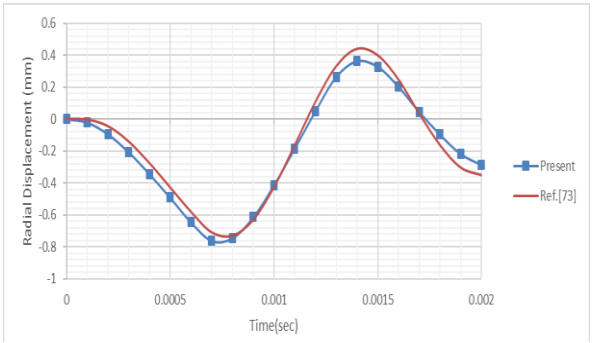

Fig.9
Comparison of temporal response of cylindrical shell with simply-supported boundary conditions $a = 0.2m$. $L = 0.2m$. $h = 1.2mm$, CFRP material, lay-up [0/90/0/90/0/90], load applying area $2l_1 \times 2l_2 = 6.2 \times 2\ cm^2$, triangular pulse type 1, $F_0 = -300kN$.

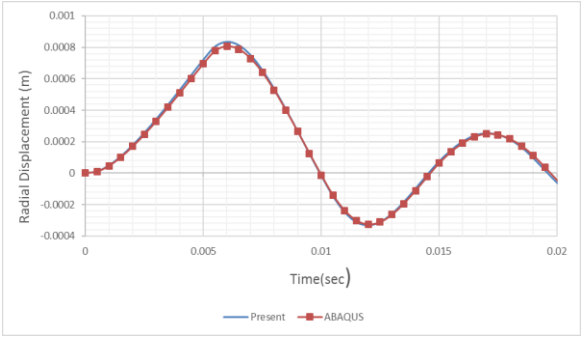

Fig.10
Comparison of the temporal response of simply-supported conical shell, CFRP material, $a = 1m$, $L = 1m$, $h = 2mm$, lay-up [0/90/0/90/0/90], load applying area, triangular pulse type 1, $f_0 = 10kPa$, 30˚-vertex angle.

11 SHELL FREQUENCY RESPONSE USING FAST FOURIER TRANSFORM

Each of the different defects that occur for rotating structures has specific vibrational characteristics. One of the important characteristics of vibration is vibrational frequency.

Usually, vibration measured from a structure is a complex signal and a combination of several vibrational signals with different frequencies. Frequency analysis, also called spectrum analysis or FFT, is a signal processing process. The frequency content of the vibrational signal is obtained using this process. In FFT curves, the horizontal axis, frequency, and vertical axis indicate the amplitude of vibration. Sometimes it is difficult to find the value of natural frequencies by looking at the temporal response diagram of a vibrational system. Using the Fourier transform, the response of the vibrational system is shifted from the time domain to the frequency domain. Then, the system frequency response spectrum is obtained [20].

Finally, the natural frequencies of the system are easily discussed. The frequency response of the studied shell in Fig. 10 is shown in Fig. 11. Frequencies stimulated by the impulse load applied to the shell can be formed in this figure. As can be seen in this figure, the predominant stimulated frequency is 97.1 *Hz*. Fig. 12 shows the natural frequencies of this shell for the number of different half-wavelengths in terms of the number of peripheral waves. As can be seen in this figure, the base natural frequency of this shell is the same as 97.1 *Hz* and occurs at $m = 1$ and $n = 11$. By applying the impulse load, the base natural frequency of the shell is more stimulated than other natural frequencies, so that the effect of the rest of the frequencies can be negligible compared to the effect of the base frequency on the temporal response.

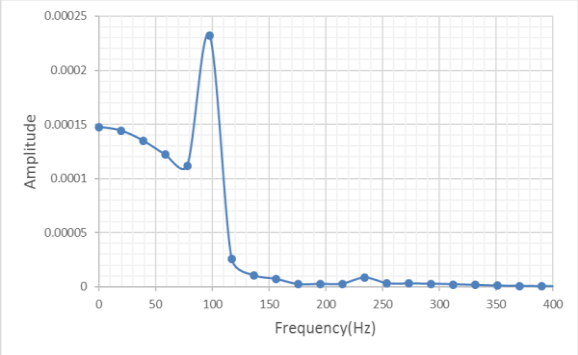

Fig.11
The frequency response of the studied shell in Fig. 10.

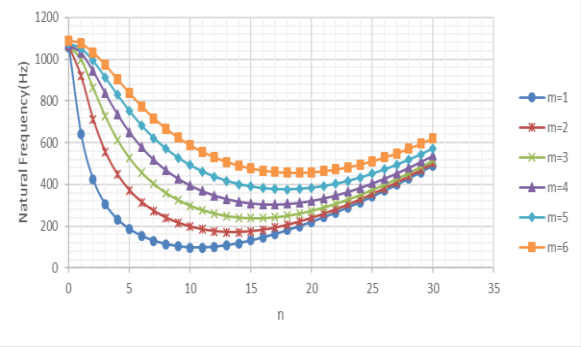

Fig.12
Natural frequencies of the simply-supported conical shell according to the number of peripheral waves, CFRP material, $a = 1m$, $L = 1m$, $h = 2mm$, lay-up [0/90/0/90/0/90], 30 ° - vertex angle.

12 PULSE PHENOMENON

As a result of applying the impact load to the shell, the pulse phenomenon occurs. Pulse phenomenon is a type of oscillation in which the amplitude of the oscillation first increases, then decreases regularly. These increase and decrease continue intermittently [19]. This phenomenon will be observed if the graph of changes in the amplitude of vibration in the radial direction is drawn to periods much larger than the natural period of the shell. This is done in Fig. 13 for a simply-supported shell.

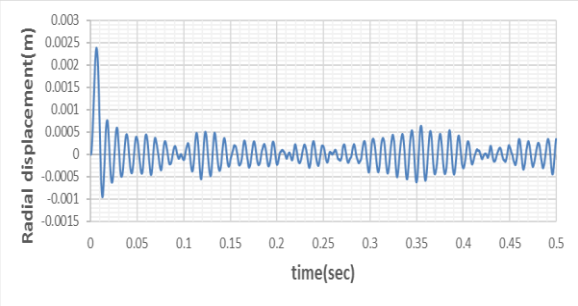

Fig.13
Presentation of the pulse phenomenon in the temporal response of the shell with simply-supported boundary conditions $a = 1m$. $L = 1m$. $h = 2mm$, CFRP material, lay-up [0/90/0/90/0/90], load applying area $2l_1 \times 2l_2 = 5 \times 5.2\ cm^2$, sine pulse type, $f_0 = 10kPa$, 30˚- vertex angle.

13 INVESTIGATING THE PARAMETERS AFFECTING THE TRANSIENT DYNAMIC RESPONSE OF THE SHELL

In Fig. 14, the radial displacement changes over time are plotted for different lay-ups using 0° and 90° angles. As can be seen, if all angles are 0° or 90°, the shell resistance to deformation will be less than when a combination of 0° and 90° angles is used together. Table 1 shows the base frequencies of the shell studied in Fig. 14 for different lay-ups.

Table 1
The base frequencies of the shell studied in Figs. (4-26)

Lay-up	[0;0;0]	[0;90;0]	[90;0;90]	[0;90;90]	[90;0;0]	[90;90;90]
Frequency (*Hz*)	62.6	65.7	95.7	77.0	71.0	76.9

Among the layouts of the layers shown in Fig. 14, the layout [90/0/90] has a minimum vibration amplitude and leads to a maximum displacement faster than other lay-ups. As mentioned, by applying the impulse load, the base natural frequency of the shell is stimulated more than other natural frequencies. The base frequency corresponding to lay-up [90/0/90] is larger than the base frequencies corresponding to other lay-ups. In fact, by increasing the base frequency value, the maximum displacement value of the shell decreases, and the temporal response of the shell becomes faster. Also, by decreasing the base frequency value, the maximum displacement value of the shell increases, and the temporal response of the shell becomes slower.

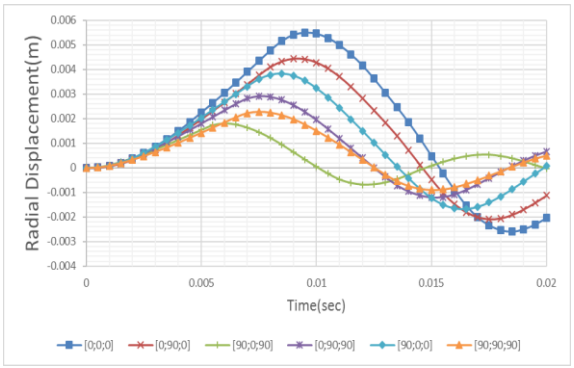

Fig.14
Effect of fiber angle on the temporal response of the shell with simply-supported boundary conditions, $a = 1m$. $L = 1m$.$h = 2mm$, CFRP material, load applying area $2l1 \times 2l2 = 5 \times 5\ cm^2$, triangular pulse type 1, $f_0 = 25kPa$, 60˚vertex angle.

14 GEOMETRIC PARAMETER EFFECT

As mentioned earlier, geometric parameters such as the ratio of thickness to the radius (h / R) and the ratio of generator length to the small radius (L / R) affect the natural frequencies of the shell. Therefore, they also affect the temporal response of the shell. Fig. 15 shows the effect of the ratio of length to shell radius on radial displacement changes over time. As can be seen, with increasing this ratio, the maximum displacement of the shell increases, so that with doubling this ratio, the maximum displacement becomes 1.37. Since with increasing this ratio, the natural

frequency decreases, the time delay of the response increases, that is, the maximum displacement of the shell occurs later. Fig. 16 shows the effect of the ratio of thickness to the radius on the changes in radial displacement over time. As shown in the figure, by increasing this ratio, the maximum shell displacement decreases. By doubling the thickness to radius ratio, from 0.004 to 0.008, the maximum displacement is reduced by 78%. Since with increasing this ratio, the natural frequency increases, the response time delay decreases, that is, the maximum shell displacement occurs earlier.

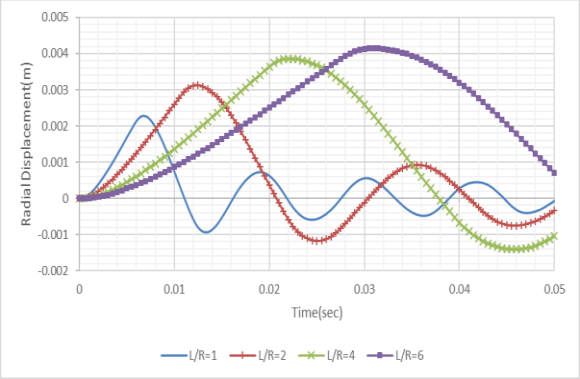

Fig.15
Effect of ratio (L / R) on temporal response of the shell with simply-supported boundary conditions, $a = 1m$. $L = 1m$. $h = 2$ mm, CFRP material, lay-up [0/90/0/90/0/90], Load applying area $2l_1 \times 2l_2 = 5 \times 5cm^2$, triangular pulse type 1, $f_0 = 25kPa$, 60˚vertex angle.

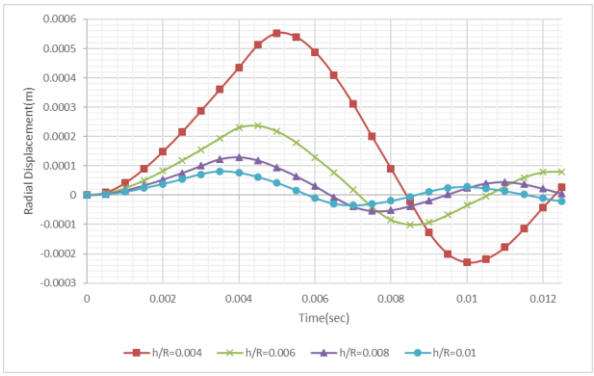

Fig.16
Effect of ratio (h / R) on temporal response of the shell with simply-supported boundary conditions, $a = 1m$. $L = 1m$. $h = 2mm$, CFRP material, lay-up [0/90/0/90/0/90], Load applying area $2l_1 \times 2l_2 = 5 \times 5cm^2$, the triangular pulse type 1, $f_0 = 25$ kPa, 60˚vertex angle.

15 INVESTIGATING THE EFFECT OF LOADING MODE ON THE TRANSIENT DYNAMIC RESPONSE OF THE SHELL

Various parameters affect the loading mode applied to the shell including the pressure change curve in terms of time (pulse type applied on the shell), duration of applied load (t_1), pressure amplitude (f_0), and location coordinates of the applied load (x_L, ϕ_L). Here, the effect of the above parameters on the transient dynamic response of the composite conical shell has been investigated.

Fig. 17 shows a graph of radial displacement changes over time, respectively, for a simply-supported shell, under the effect of five types of step, sine, triangle 1, triangle 2, and triangle 3 pulses, respectively. By comparing the responses related to the different pulses, it can be seen that the maximum displacement of the shell corresponding to any pulse which has more area below the curve, is greater than others. In the case of triangular pulses 2 and 3, which have the same area below the curve, it is important to note that the maximum displacement corresponding to triangular pulse 2, is larger than triangular pulse 3. This is because, in a triangular pulse 3, the load starts from zero and gradually increases, but in a triangular pulse 2, the load at zero time immediately jumps from zero to f_0. Therefore, the inertia (mass-induced inertia) of the shell is not able to withstand this drastic load change.

Fig. 18 shows the continuous pulse and its effect. As shown in the diagram, due to the continuous pulse, no oscillation occurs around the zero strain. However, this pulse leads to a maximum allowable radial strain at a much lower pressure.

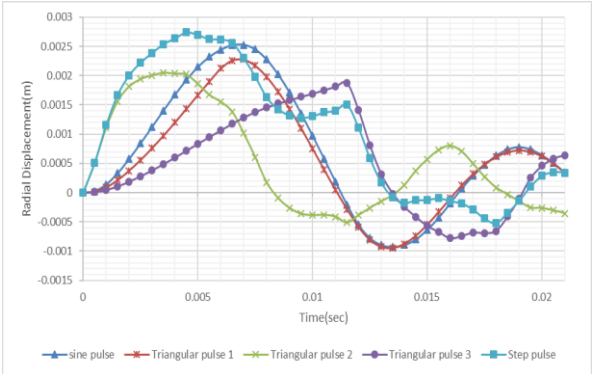

Fig.17
Comparison of radial strain changes of different pulses with time for the shell with simply-supported boundary conditions, a =1m. L =1m. h =2mm, CFRP material, lay-up [0/90/0/90/0/90], Load applying area $2l_1 \times 2l_2 = 5 \times 5\ cm^2$, f_0 = 25kPa, 60˚vertex angle.

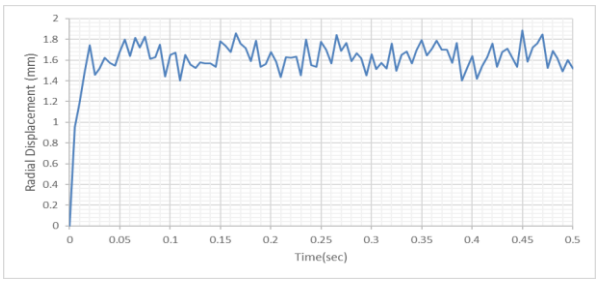

Fig.18
Radial strain changes of the continuous pulse with time for the shell with simply-supported boundary conditions, a =1m. L =1m. h = 2mm, CFRP material, lay-up [0/90/0/90], Load applying area $2l_1 \times 2l_2 = 5 \times 5cm^2$, f_0 = 20kPa, 60˚vertex angle.

16 THE EFFECT OF THE DURATION OF THE APPLIED LOAD

Fig. 19 shows the effect of the change in the duration of the applied load on the shell (t_1) on the changes in the radial displacement of the shell over time. As can be seen, if this duration is close to the natural period of the shell (N.P.), which is equal to 0.0115 s, the maximum displacement of the shell will be greater. If the duration of applied impact load is close to the normal period, the mode shape corresponding to the base frequency, and other mode shapes corresponding to the frequencies close to the base frequency, are further stimulated. As a result, the movement will be increased.

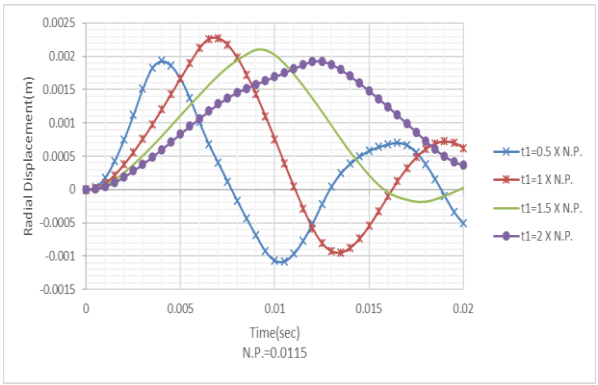

Fig.19
The effect of the duration of the applied impulse load (as a multiple of natural periods) on the surface of the shell with simply-supported boundary conditions, a =1m. L =1m. h = 2mm, triangular pulse type 1, CFRP material, lay-up [0/90/0/90/0/90], load applying area $2l_1 \times 2l_2 = 5 \times 5\ cm^2$, f_0 = 25kPa, 60˚vertex angle.

16.1 Load amplitude effect

Fig. 20 shows the effect of the maximum amount of applied load (f_0) on the shell on radial displacement changes over time. As can be seen in this figure, by changing the amount of applied load f_0, only the size of the vibration amplitude changes. This change has no temporal effect on the displacement variation diagram (because the natural frequencies have not changed). Also, the size of the resulting vibration amplitude has a direct and linear relationship with the value of f_0.

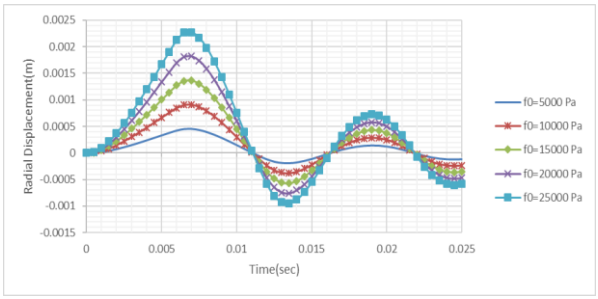

Fig.20
The Effect of f_0 value on radial displacement changes of the shell with simply-supported boundary conditions over time, $a = 1m$. $L = 1m$. $h = 2mm$, triangular pulse type 1, CFRP material, lay-up [0/90/0/90/0/90], load applying area $2l_1 \times 2l_2 = 5 \times 5\ cm^2$, $f_0 = 25kPa$, 60˚vertex angle.

16.2 Effect of location coordinates of the applied load

Fig. 21 shows the effect of the location coordinate of the applied load (x_L, Θ_L) on radial displacement changes over time. As shown in this figure, the closer the location coordinates of the applied load are to the coordinates of the point at which we calculate the displacement ($x = L/2$, $\theta = 0$), the greater the maximum displacement value of that point. Thus, it is concluded that the farther the location of the applied load is from the point of interest for calculating the temporal response, the later the maximum displacement of that point occurs. The reason for this delay is the wave propagation in a continuous medium (conical shell). Wave propagation speed is limited in a continuous medium. So, it takes a while to move from one point to another.

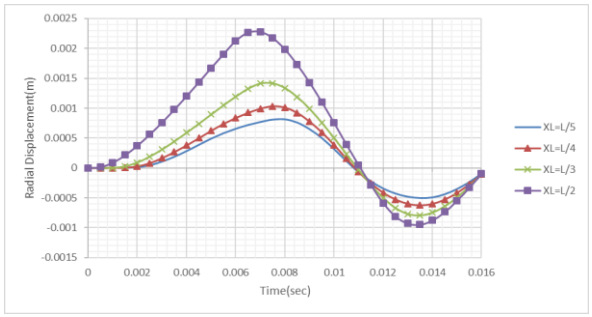

Fig.21
The effect of impact load location $x = x_L$.$\Theta = 0$ on radial displacement changes of simply-supported shell over time, $a = 1m$. $L = 1m$. $h = 2mm$, triangular pulse type 1, CFRP material, lay-up [0/90/0/90/0/90], Load applying area $2l_1 \times 2l_2 = 5 \times 5\ cm^2$, 60˚vertex angle.

16.3 The effect of the vertex angle of the cone

As shown in Fig. 22, by increasing the vertex angle of the cone, due to the decrease in natural frequency, the maximum displacement of the shell increases. As a result, the time delay of the response increases, and the maximum displacement of the shell occurs later.

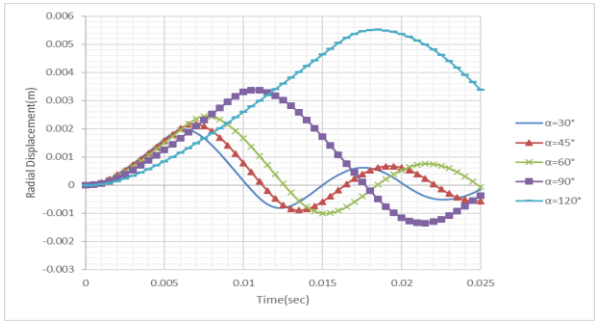

Fig.22
The effect of the cone vertex angle on radial displacement changes of simply-supported shell over time, triangular pulse-type 1, CFRP material, lay-up [0/90/0/90/0/90], $a = 1$ m. $L = 1m$. $h = 2mm$, load applying area $2l_1 \times 2l_2 = 5 \times 5\ cm^2$.

16.4 Effect of orthotropic ratio

According to Fig. 23, the behavior of composites with higher orthotropic ratios is closer to the behavior of isotropic materials, and this parameter has a great effect on the amount of impulse-induced displacement.

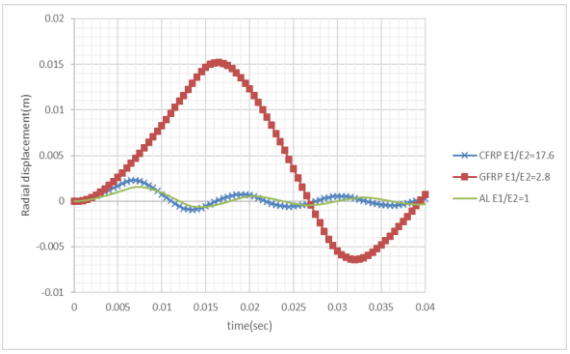

Fig.23
The effect of material orthotropic ratio on radial displacement changes of simply-supported shell over time, $a = 1m$. $L = 1m$. $h = 2mm$, triangular pulse-type 1, lay-up [0/90/0/90/0/90], Load applying area $2l_1 \times 2l_2 = 5 \times 5cm^2$, 60° vertex angle.

17 VERIFICATION

Figs. 24 and 25 show the results of the computer code obtained from the ABAQUS finite element software. Besides, by adding horizontal ribs that make the stiffener grid denser, the results of the calculations based on the theory of the present study are closer to the results of the finite element software. This shows that the denser the grid, the more valid the equivalence method is.

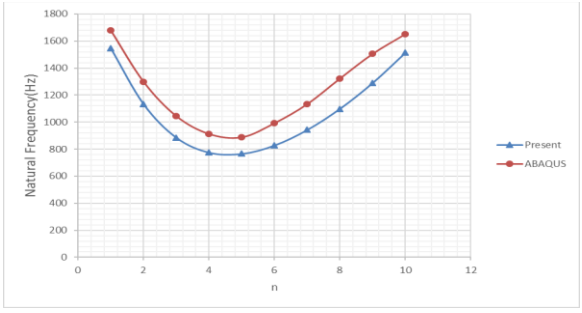

Fig.24
Comparison of the natural frequency of grid-stiffened structure without horizontal rib.

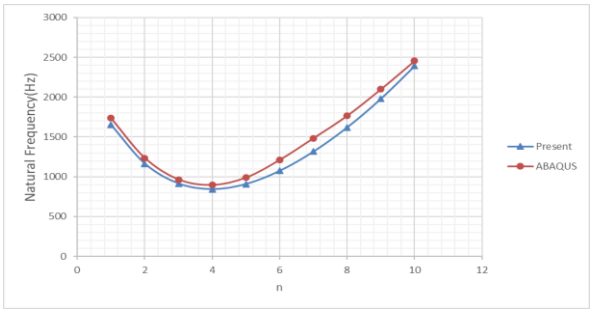

Fig.25
Comparison of the natural frequency of grid-stiffened structure with horizontal rib.

The mode shapes obtained from the analysis in Fig. 26, is shown below.

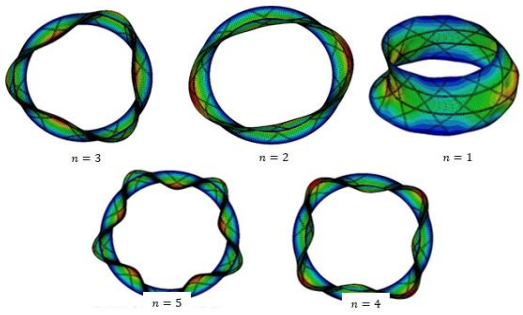

Fig.26
Mode shapes obtained from the modal analysis of composite grid-stiffened conical shell $m = 1$.

18 INVESTIGATING THE EFFECT OF ADDING STIFFENER TO STRUCTURES WITH THE SAME MASS

The masses of the conical shell (with and without stiffener) are considered constant values and the natural frequency and the structure response to the transient dynamic load are investigated.

Fig. 27 shows that adding a stiffener increases the natural frequency and base frequency of the system. Also, Fig. 28 shows that by increasing the base frequency corresponding to the stiffened shell, the maximum displacement of the shell decreases, and the temporal response of the shell becomes faster. Also, the base frequency increases and occurs in a lower mode ($n = 4$). The modified specifications in this comparison are given in Table 2.

Table 2
Specifications of the conical shell with and without stiffener with the same mass.

Type	Stiffener thickness	Shell thickness	
CFRP	6	1	Shell with stiffener
CFRP	0	2.56	Shell without stiffener

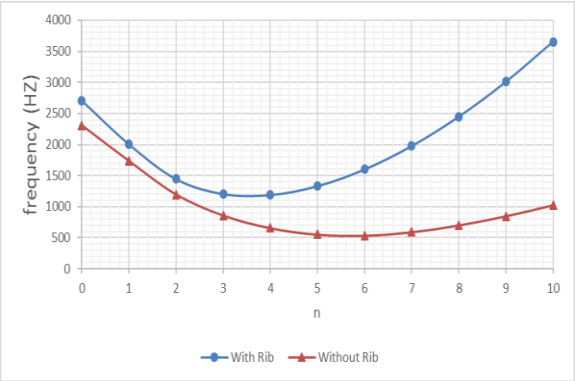

Fig.27
Comparison of the natural frequency of the conical shell with and without stiffener, m =1.

Adding a stiffener reduces the maximum displacement of the shell by 25% against transient dynamic loading where the mass of both structures is the same.

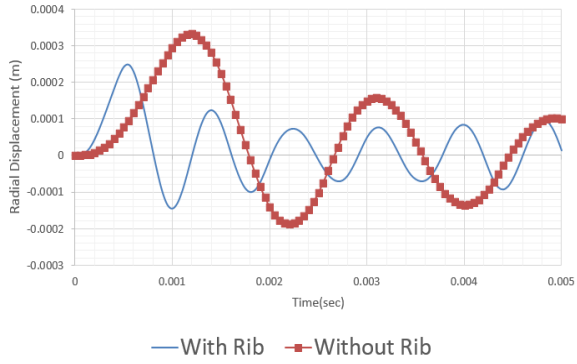

Fig.28
The effect of stiffener on radial displacement changes of simply-supported conical shell over time, triangular pulse-type 1, $f_0 = 25kPa$.

19 EXAMINING THE STIFFENER HEIGHT CHANGES

The effect of increasing the height of the rib (H) is shown in Figs. 29 and 30. As the thickness increases, the natural frequency increases in the modes higher than the base natural frequency. Also, an increase in the thickness of the stiffener reduces the maximum displacement of the shell.

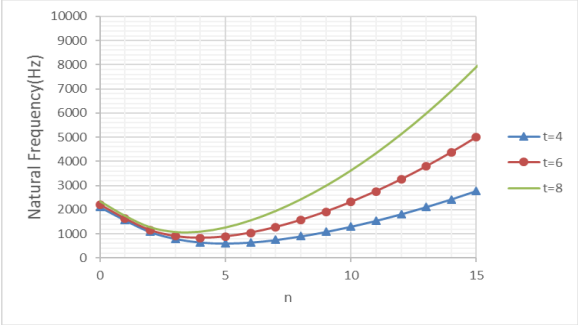

Fig.29
Effect of increasing rib height (H) on the natural frequency of conical grid-stiffened shell, $m = 1$.

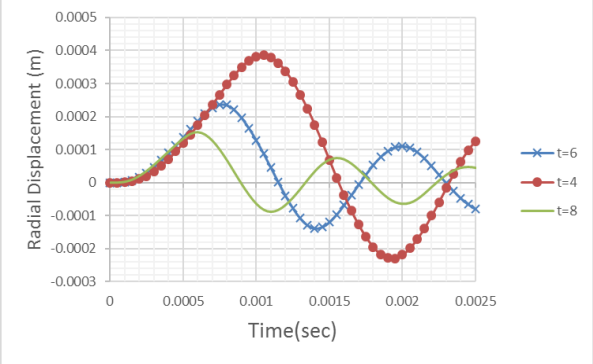

Fig.30
The effect of increasing the height of the rib (H) on the radial displacement changes of the grid-stiffened simply-supported conical shell over time, triangular pulse-type 1, $f_0 = 25kPa$.

20 INVESTIGATING THE CHANGE OF UNIT CELL DIMENSIONS

Two sets of the unit cells, A and B, with the properties listed in Table 3 have been investigated. As can be seen from the calculated volume fraction, with decreasing the dimensions of the unit cell and increasing the stiffener density, the volume fraction of the stiffener is increased. Comparing the results in Fig. 31 shows that increasing the density of stiffeners increases the natural frequency, especially at high modes. Fig. 32 also shows that increasing the density of the stiffeners reduces the maximum displacement of the shell.

Table 3
Parameters of cell units.

	ast	bst	Vst	Vst
A	138	153	0.44	0.56
B	69	67.5	0.58	0.42

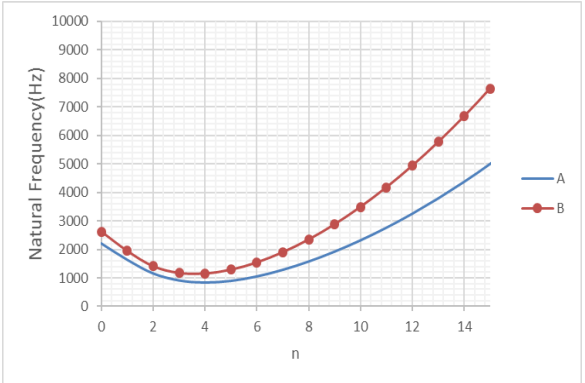

Fig.31
The effect of increasing the stiffener density on the natural frequency of the grid-stiffened conical shell, $m = 1$.

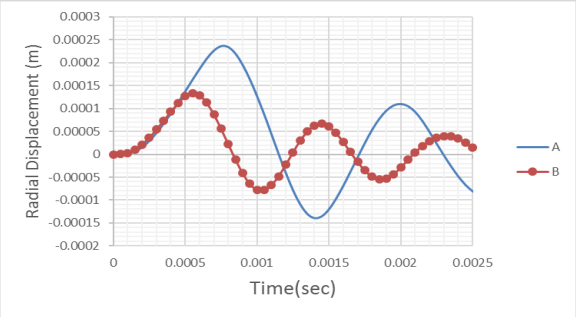

Fig.32
Effect of increasing stiffener density on radial displacement changes of grid-stiffened simply-supported conical shell over time, triangular pulse-type 1, $f_0 = 25kPa$.

21 CONCLUSIONS

The transient dynamic response of a composite conical shell with simply-supported boundary conditions is influenced by various parameters such as fiber angle, layer arrangement, thickness to radius ratio, length to radius ratio, orthotropic ratio, loading mode, and the vertex angle of the cone. The effect of these parameters is as follows:

- A certain combination of angles of 0° and 90° degrees can be found in which the maximum amplitude of the shell vibration is the lowest possible value.
- As the length-to-radius ratio increases, the amplitude of the shell vibration increases. As a result, the maximum amplitude of the shell vibration occurs later.
- As the thickness-to-radius ratio increases, the amplitude of the shell vibration decreases. As a result, the maximum amplitude of the shell vibration occurs earlier.

In general, with increasing the base frequency value, the maximum value of the shell vibration amplitude decreases, and the shell temporal response becomes faster. Also, as the base frequency decreases, the maximum value of the shell vibration amplitude increases and the time response of the shell slows down. Besides, the temporal response frequency is equal to the same base frequency. Thus, increase or decrease in the base frequency value may be due to various reasons such as changes in the arrangement of the layers, changes in the ratio of length to the radius, changes in the ratio of thickness to the radius, changes in the vertex angle of the cone, and so on.

Among the various pulses applied to the shell, the step pulse causes more deformation in the shell. This is due to the more area below the diagram corresponding to the step pulse. If the duration of applying the impulse load is close to the natural period of the structure, the amplitude of the shell vibration will be increased. The reason is that the mode shape amplitude corresponding to the base frequency is higher and as a result, the base frequency is stimulated more than other frequencies. The shell vibration amplitude under the influence of the impulse load changes linearly as the load size changes. After applying an impact load, the points far from the load applying area reach their maximum vibration amplitude later than the points close to the load applying area. The use of grid stiffeners affects the natural frequency and transient dynamic response of the composite conical shell. The results of the studies are as follows:

- In equating the grid-stiffened composite conical shell, the higher the grid density, the closer the results of this equivalence theory are to the results of the finite element software.
- By equating the stiffness matrix of a grid-stiffened composite conical shell and comparing it to a composite conical shell of the same mass, the natural frequency increases and its effect is more pronounced in a large number of peripheral waves (n). Also, the shell vibration amplitude is reduced and the temporal response of the shell becomes faster.
- Increasing the thickness of the stiffener and the density of the stiffener grid increases the natural frequency and reduces the vibration amplitude of the grid-stiffened composite conical shell.

REFERENCES

[1] Dobyns A. L., 1981, Analysis of simply-supported orthotropic plates subject to static and dynamic load, *AIAA Journal* **19**: 642650.
[2] Ramkumar R. L., Chen P. C., 1983, Low-velocity impact response of laminated plates, *AIAA Journal* **21**: 1448-1452.
[3] Cederbaum G., Heller R. A., 1989, Dynamic deformation of orthotropic cylinders, *Transactions of the ASME, Journal of Pressure Vessel Technology* **11**: 97-101.

[4] Reddy J.N., Khdeir A.A., 1989, Dynamic response of cross-ply laminated shallow shells according to a refined shear deformation theory, *The Journal of the Acoustical Society of America* **85**: 2423-2431.
[5] Davar A., 2009, Analysis and optimization of laminated composite circular cylindrical shell subjected to compressive axial and transverse transient dynamic loads, *Thin-Walled Structures* **47**: 970-983.
[6] Davar A., 2010, Dynamic response of pre-stressed fiber metal laminate (FML) circular cylindrical shells subjected to lateral pressure pulse loads, *Composite Structures* **92**: 1308-1317.
[7] Jaunky N., Knight N.F., Ambur D.R., 1998, Optimal design of general stiffened composite circular cylinders for global buckling with strength constraints, *Composite Structures* **41**: 243-252.
[8] Wang J.T.S., Hsu T.M., 1995, Discrete analysis of stiffened composite cylindrical shells, *AIAA Journal* **23**: 1753-1761.
[9] Kidane S., Li G., Helms J., Pang S., Woldesenbet E., 2003, Buckling load analysis of grid stiffened composite cylinders, *Composites Part B: Engineering* **34**: 1-9.
[10] Wodesenbet E., Kidane S., Pang S., 2003, Optimization for buckling loads of grid stiffened composite panels, *Composite Structures* **60**: 159-169.
[11] Yazdani M., 2009, *Analytical and Experimental Buckling Analysis of Grid Stiffened Composite Shells under Axial Loading*, Ph.D. Dissertation, Tarbiat Modares University, Iran.
[12] Yazdani M., Rahimi G.H., Afaghi Khatibi A., Hamzeh S., 2009, An experimental investigation into the buckling of GFRP stiffened shells under axial loading, *Scientific Research and Essays* **4**: 914-920.
[13] Yazdani M., Rahimi G.H., 2010, The effects of helical ribs' number and grid types on the buckling of thin-walled GFRP stiffened shells under axial loading, *Journal of Reinforced Plastics and Composites* **29**: 2568-2575.
[14] Yazdani M., Rahimi G.H., 2011, The behavior of GFRP-stiffened and -unstiffened shells under cyclic axial loading and unloading, *Journal of Reinforced Plastics and Composites* **30**: 440-445.
[15] Rahimi G.H., Zandi M., Rasouli S.F., 2013, Analysis of the effect of stiffener profile on buckling strength in composite isogrid stiffened shell under axial loading, *Aerospace Science and Technology* **24**: 198-203.
[16] Hemmatnezhad M., 2014, On the free vibrations of grid-stiffened composite cylindrical shells, *Acta Mechanica* **225**: 609-623.
[17] Davar A., 2003, *Vibrations of Composite Cylindrical Shells*, M.Sc. Thesis, Khajeh Nasir al-Din Tusi University of Technology.
[18] Yong-shin L., Ki-Du L., 1997, on the dynamic response of laminated circular cylindrical shell under impulse loads, *Computers & Structures* **63**(1): 149-157.
[19] Rao S.S., 1985, *Mechanical Vibration*.
[20] Thomson W.T., 1988, *Theory of Vibration with Application*, Englewood Cliffs.